

The impact of a contractile actomyosin system on reconstituted phase separated membranes

Der Einfluss eines kontrahierenden Aktomyosin Systems auf
rekonstituierte phasenseparierte Membranen

MASTERARBEIT

zur Erlangung des akademischen Grades
Master of Science
(M. Sc.)
im Fach Biophysik



eingereicht an der
Mathematisch-Naturwissenschaftlichen Fakultät I
Institut für Biologie
Humboldt-Universität zu Berlin

von
Ferdinand Greiss
geboren am 03.12.1986 in München

Betreuung:

1. *Prof. Dr. Andreas Herrmann*
2. *Prof. Dr. Petra Schwille*

eingereicht am: 01.Mai 2013

Zusammenfassung

Das Flüssig-Mosaik-Modell, einst von Seymour Jonathan Singer und Garth Nicolson im Jahre 1972 entworfen, wird mit der Erweiterung der lateralen Selbstorganisation in Form von Mikrodomänen dem eigentlichen Zellverhalten näher gebracht. Durch die Verankerung von Actinfilamenten durch eine Vielzahl von Membranproteinen an die Innenseite der Plasmamembran, wurde die Membranorganisation teilweise dem Actincortex zugeschrieben.

Um den aktiven Einfluss eines dynamischen Actincortexes auf die Membranorganisation genauer zu studieren, wurde im Rahmen dieser Masterarbeit ein Minimalsystem, bestehend aus Aktomyosin und einer phasenseparierten Membran (3:3:1 DOPC/PSM/Cholesterol), entwickelt. FRAP Experimente zeigten eine langsame Bewegung des biotinylierten Lipids DSPE über die Grenzlinie der makroskopischen flüssig-geordneten und flüssig-ungeordneten Domänen. Durch die Anlagerung der Actinfilamente an die Membran mit Hilfe von DSPE, haben wir Grund zu der Annahme, dass das langsame Diffusionsverhalten dieser Verankerungen Einfluss auf das Kontraktionsverhalten und der Membranorganisation nimmt. Wie wir mit Interner Totalreflexionsfluoreszenzmikroskopie beobachten konnten, wurde die Kontraktion des Actinnetzwerkes durch ATP-konsumierende Myosin-Filamente an den Phasengrenzlinien gehindert. Die gehinderte Bewegung führte zur Domänenverformung und zur gerichteten Bewegung der Actinfilamente entlang der Phasengrenzlinien. Für den Fall, dass flüssig-geordnete Domänen nahe aneinander lagen, führte die Verformung zur Verschmelzung. Weiter konnten wir zeigen, dass verformte Domänen zurück in ihre Ausgangsposition relaxierten sobald sich F-Actin von der Phasengrenzlinie entfernte.

Die Domänenverformung wurde quantitative mit di-4-ANEPPDHQ und einem vereinfachten aktiven Kontur-Algorithmus analysiert. Während der Domänenverformung konnte keine Änderung der Packungsordnung mit di-4-ANEPPDHQ, jedoch ein Flächenzuwachs der flüssig-geordneten Domänen mit dem aktiven Kontur-Algorithmus gezeigt werden.

Diese Ergebnisse können entscheidend für das Verständnis zellulärer Prozesse, sowohl im Bereich der Signaltransduktion wie auch der Zellmorphogenese, genutzt werden.

Schlagwörter:

Minimalsystem, Phasenseparierte Membrane, Actincortex, Mikrodomänen, Signaltransduktion, Zellmorphogenese

Contents

1	Introduction	1
1.1	Membranes & Actin Cortex	1
1.1.1	Membrane Organization	2
1.1.2	Actincortex in Cells	6
1.2	Project Aims	8
2	Materials and Methods	9
2.1	Chemicals	9
2.2	Proteins	9
2.2.1	Actin Labeling and Polymerization	9
2.2.2	Rabbit Muscle Myosin II Purification	10
2.2.3	Dialysis of Myofilaments for Length Determination	10
2.3	Minimal Actin Cortex Assembly	10
2.4	Microscopy	13
2.4.1	Atomic Force Microscopy	13
2.4.2	Total Internal Reflection Microscopy	13
2.4.3	Laser Scanning Microscopy	14
2.5	Data Analysis	14
2.5.1	Software	14
2.5.2	Analysis of di-4-ANEPPDHQ data	15
2.5.3	FRAP Analysis	15
2.5.4	Simplified Active Contour Algorithm	16
3	Results	17
3.1	Minimal Actin Cortex Assembly on Phase Separated Membrane . . .	17

3.2	Length Distribution of Equilibrated Myofilaments	19
3.3	Dynamic Behavior of the Biotinylated Lipid DSPE	20
3.4	Deformation of Phase Boundaries by the Contractile Actomyosin Network	22
3.5	Quantitative Analysis of Phase Deformation	27
4	Conclusion and Future Prospects	30
4.1	Length Distribution of Equilibrated Myofilaments	30
4.2	Contractile Behavior of Actomyosin on Phase Separated Membranes	30
4.2.1	Mechanistic Observations at the Phase Boundary	30
4.2.2	Models for Area Growth of Phases	32
4.3	Biological Implications & Future Investigations	33

List of Figures

1.1	Illustration of membrane organization	3
1.2	Phase separated membranes form various shapes	4
1.3	Schematic illustration of the three main lipid packing orders	5
1.4	Myofilament with sliding filamentous actin on single myosin heads	7
2.1	Illustration of assembled minimal actin cortex on lipid bilayer without support	12
3.1	Contraction of medium dense actin network on phase separated membrane was induced by the addition of myosin motors and ATP	18
3.2	Length distribution of myofilaments which were equilibrated in various KCl concentrations and measured with atomic force microscopy	19
3.3	FRAP analysis was performed on phase separated membrane in order to characterize DSPE diffusion	21
3.4	Accumulation of F-actin asters at phase boundary	22
3.5	Probability tree of deformation events during actomyosin contraction	23
3.6	Example for the extrusion event of liquid ordered phases	24
3.7	Example for indentation events of liquid ordered phases	25
3.8	Example for relaxation events of phase boundary after actin filament dissociation	26
3.9	Quantitative imaging of phase deformation by actomyosin contraction with di-4-ANEPPDHQ	27
3.10	Active contour algorithm applied to a simple deformation event	28
4.1	Schematic illustration of actomyosin contraction on phase separated membran	31

Chapter 1

Introduction

1.1 Membranes & Actin Cortex

The self-organization of living membranes by lipid-lipid, lipid-protein and protein-protein interactions extends the former model of the fluid-mosaic membrane model introduced by Seymour Jonathan Singer and Garth Nicolson in the year 1972. Active regulation of membrane associated events in temporal and spatial space is further provided by the highly conserved protein actin. The rearrangement of membrane bound actin filaments - the actin cortex - is known to lead to the reorganization of membrane proteins, which are either directly attached or associated as for instance small G proteins:

Several studies showed that filamentous actin (F-actin) is regulating the clustering of small G proteins in the membrane by interacting with lipid rafts. This family of signalling proteins is not only responsible for cell morphogenesis, but also for numerous developmental and survival programs [2].

Both cell components - the actin cortex and membrane organization - overlap frequently in appearance when it comes to signal regulation or cell morphogenesis. Numerous studies have been published for each of them, but only few were concerned about their mutual importance. Within the scope of this study we were trying to reveal the underlying connections of the actively rearranging actin cortex

and the membrane organization, known as lipid rafts, *in vitro*.

1.1.1 Membrane Organization

Introduction to Lipid Rafts

The spatial integrity of living cells is maintained by the plasma membrane, which separates intracellular from extracellular space. Further partitioning into subcompartments, named organelles, by lipid bilayers within the cell confine and concentrate biochemical reactions. All those hurdles need to be controlled in order to communicate for the bigger good of cell adaption and life in the natural environment. About one-third of all proteins encoded by the genome spend therefore part of their lifetime at the membrane [19]. The lateral organization of the densely packed bilayer is argued to be controlled by a physical and chemical membrane heterogeneity in form of lipid rafts. The size (20-100 nm [10]) and lifetime of rafts are with the order of nanometers and microseconds at the limit of what can be resolved by standard microscopy techniques. Their functional role *in vivo* is therefore one of the most controversial subjects in biological science nowadays.

Activated, clustered lipid rafts are supposed to consist primarily of three different lipid classes. Sterol as one of them being present in all higher organisms and in mammals specifically in the form of cholesterol. Sphingolipid as the second member is based on ceramide and is found mostly as sphingomyelin or glycosphingolipid. The third component is suggested to be membrane-associated proteins, which upon activation by biochemical signals may form highly ordered networks. Rafts in their active state are thought to subcompartmentalize the biological membrane by coalescing proteins and lipids according to their preferences for membrane order and chemical interactions [19].

Further accumulation to large lipid raft clusters is however argued to be hindered by a myriad of factors one of them being the dynamic actin cortex. By changing the diffusion behavior of lipids and proteins, the cortex prevents the global phase separation as observed in equilibrated artificial membranes [9][6].

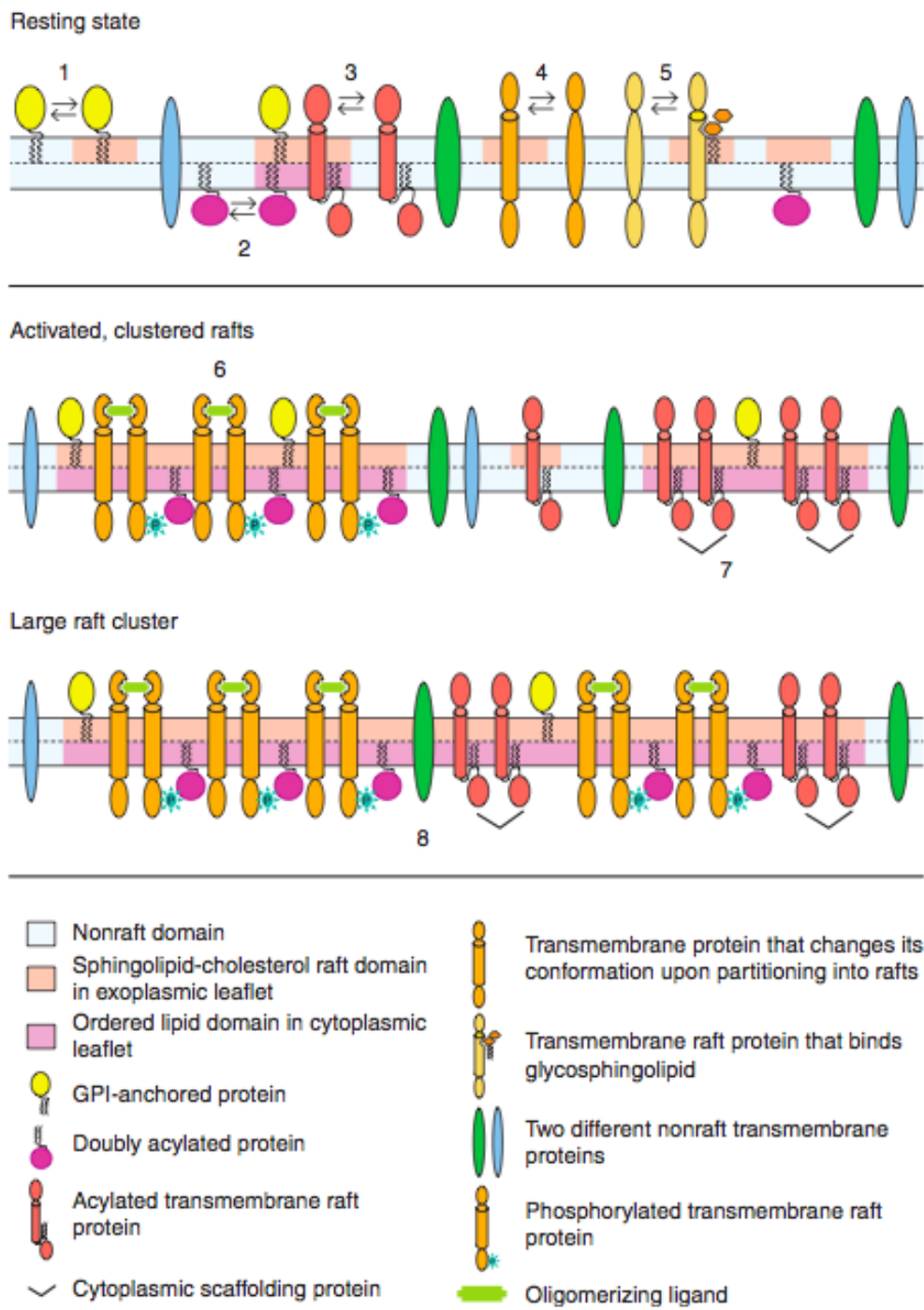


Figure 1.1: Illustration of freely diffusing membrane proteins for the case of a homogeneous membrane in the resting state. Active rafts are obtained by clustering proteins through activation, which may lead to conformational changes, binding to raft associated sphingomyelins or cross-linkage. Spatial organization of proteins is provided by internal scaffolding proteins. The accumulation of various raft proteins results in large clusters capable of signal regulation [19].

It has been reported that under specific circumstances membrane proteins in biological systems recruit lipids from the vicinity, “leading to the formation of greater, stabilized rafts with lifetimes longer than several min [11]”. Those long living raft clusters are assumed to be key players in signal propagation. By regulating the lateral organization of membrane signaling proteins, the cell is able to either diminish or promote signals passing the membrane in spatial and temporal space.

The lateral heterogeneity in biological membranes is however not only assumed to be involved in signal regulation, but also in shape remodeling. As single lipids deviate from cylindrical shapes and aggregate, an initially plane membrane becomes positively or negatively curved. The membrane deformation may induce a starting point for budding and fission with the help of osmotic pressure or shape-inducing external proteins as several studies suggest [10].

Evidence for a functional role of lipid rafts in cell morphogenesis was also found experimentally in the fission yeast *Schizosaccharomyces pombe*.

Relocalisation of rafts from cell poles to the fission site during mitosis was observed with the help of the polyene antibiotic filipin. The fluorescent probe forms specific complexes with cholesterol which is claimed to be associated with liquid ordered membrane domains [16].

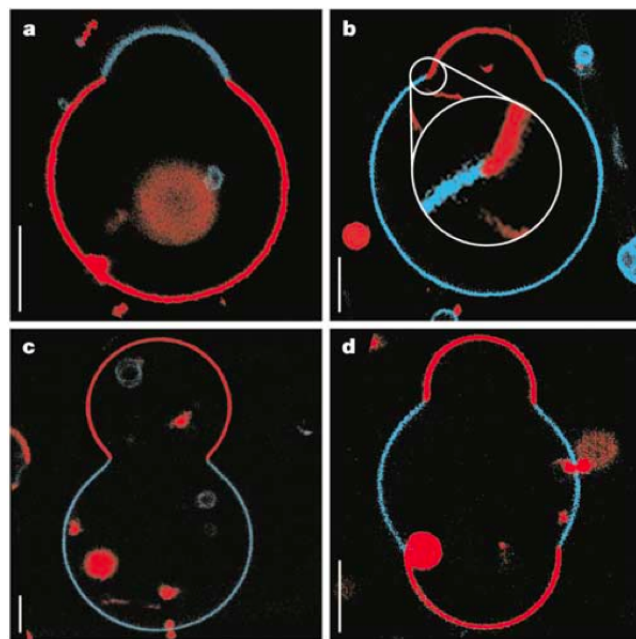


Figure 1.2: Artificial lipid bilayers are used frequently for mimicking lipid rafts in biological systems. Giant unilamellar vesicles with coexisting macroscopic liquid ordered and disordered phases form various shapes. L_o domains were labelled with perylene (blue) and L_d phase with rho-DPPE (red). Scale bar, $5\mu\text{m}$. Image taken from [3].

Introduction to Phase Separated Membranes

The phase separation of ternary lipid mixtures has been used for several years as a minimal system of membrane organization. Even though phase separation in artificial systems is difficult to compare with the lateral organization of membranes in living organisms, it has still validity due to its ease and straight forward approach to measure otherwise non accessible parameters. Artificial lipid mixtures below the melting temperature and within a relative concentration range show a demixing tendency into coexisting macroscopic lipid phases.

As several studies dealt with the theoretical foundation of phase separation in lipid mixtures, it is now known that the jump and transition ($L_o \rightarrow L_d$ and vice versa) probability of single lipid molecules under thermodynamic pressure result in the global separation of lipid molecules at specific temperature and pressure levels [6]. Physical differences, e.g. melting temperature, acyl chain saturation degree and chain length of lipid species in the system describe parameters for the tendency of phase separation.

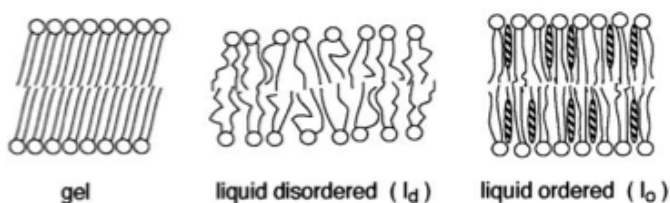


Figure 1.3: Schematic illustration of the three main lipid packing orders. Lipids below the melting temperature form highly ordered bilayer and undergo a transition from gel to liquid disordered state if they exceed T_m . The liquid ordered state is reached by fluidizing the gel phase through intercalating cholesterol [13].

These phases are categorized under three main packing states: liquid ordered (L_o), liquid disordered (L_d) and solid ordered (S_o or gel) phase. Lipids undergo a transition from solid ordered to disordered packing states as the characteristic melting temperature is passed. The gel phase is described by a highly ordered lipid phase where acyl chains form elongated and compact structures resulting in a thicker membrane compared to liquid lipids. The intermediate state of both is described by the term liquid ordered and may be formed by the presence of

intercalating cholesterol [13].

1.1.2 Actincortex in Cells

Bound to the inner side of the plasma membrane by a variety of membrane proteins, the thin actin network maintains the physical integrity of eukaryotic cells. The cortex as mechanical scaffold consists of actin filaments, myosin motors and actin-binding proteins. Rearranging the complex cortical actin mesh during dynamic cell processes in the time range of seconds is achieved by constant polymerization and depolymerization. Monomeric actin (G-Actin) becomes for these purposes filamentous forming a isotropic superstructure with mesh sizes from 20 to 250 nm beneath the plasma membrane. Most of the proteins orchestrating the steady-state properties of the actin cortex still operate in the shadow. The only class extensively studied is the actin-binding protein group - the filamins. Genomic deletion leads to the loss of shape control and organization of membrane domains [21].

The mechanical properties of the cortex are similar to a elastic solid on a macroscopic level. On a molecular level, actin filaments can be described as semi flexible polymers (persistence length¹ of 10-15 μm) which break under a certain amount of compressive stress as recently published [23]. The dynamic structure of cells, which is needed for cell adaption, locomotion or growth, is maintained by continuous turnover of actin cortex components. The limiting bottleneck of cortex remodeling pose the turnover rate of crosslinks as observed with the overexpression of the crosslinking protein α -actinin [17].

The importance of the ATP-dependent motor protein myosin for actin, one of its most numerous cited partner in scientific publications beside the terms “animals”, “muscles” and “proteins” [1], is indisputable. Single myosin proteins wan-

1

$$\langle \hat{t}(s) \cdot \hat{t}(0) \rangle = e^{-s/P} \quad (1.1)$$

\hat{t} = unit tangent vector to chain at position s , P = persistence length

der along actin filaments by tilting and wobbling its two actin-binding heads. The hydrolyzation of ATP initiates rebinding to actin after stroking, beginning the next biochemical reaction cycle [4]. The unidirectional motion as caused by polar actin filaments is used for cargo transportation between the inner cell space and the plasma membrane as it happens during e.g. exocytosis. Due to the intrinsic helical structure of F-actin, the step size of myosin heads, which differs significantly among myosin family members, is argued to be important for linear movement. Spanning the helical repeat of actin, myosin would wander straight. Otherwise, rotational mobility has to be taken into account [24].

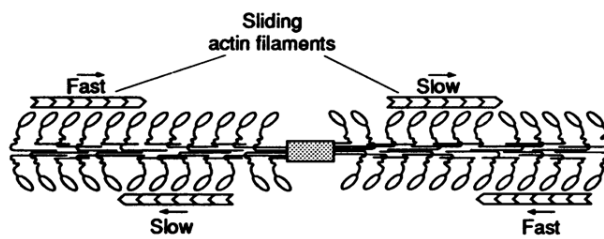


Figure 1.4: Myofibril with sliding filamentous actin on single myosin heads. Myosin II is arranged in an antiparallel fashion connected by a bare zone (crosshatched area). Fast and slow motion of actin depends on relative orientation of myosin heads and actin polymers [18].

While wandering along a single actin filament hydrolyzing ATP, both ends are described by their different mobility as leading and trailing end. The relative motion of the myofibril poles bound to two parallel aligned actin filaments results therefore in a net dragging force generated by the leading end. The contraction on single F-actin polymers in contrast was recently introduced as a global mechanism for actin turnover. The study argued that single myofibrils have the ability to bend and break membrane-bound actin filaments at low ATP levels maintaining the monomeric actin pool [23].

For the specific case of unipolar and nonprocessive myosin II proteins, it is known that tail domains promote the accumulation to a highly processive bipolar complex named myofibril as seen in figure 1.4. Multiple non-muscle myofibrils account for the contractility of the actin cortex during shape remodeling or of the mitotic ring during cytokinesis. The structure consists of two antiparallel locomotive parts at the filament ends connected via a bare zone [18].

1.2 Project Aims

The published work of Liu et al. [12] describe the influence of branched actin networks on the phase separation in giant unilamellar vesicles. The formation of localized actin networks by the Arp2/3 protein on PIP₂-containing vesicles was shown to act as switch for spatial and temporal membrane organization. The reversible process of phase aggregation was observed by changing the temperature upon actin network growth. The influence of *actively* rearranging actin networks by myosin motors on the organization of membranes has however not been yet investigated. The combination of phase separated membranes and a contractile actin cortex both reconstituted *in vitro*, provides a minimal system in order to reveal the active role of dynamic actomyosin remodeling for membrane organization.

The dragging of anchor proteins over the boundary of lipid phases by rearranging actin may excite force to the bilayer under the premise of a diffusive energetic barrier between lipid rafts and the bulk phase. The impact factor would most likely depend on the hopping properties of the actin-bound membrane protein between liquid ordered and disordered phases as well as on the dynamics of actin rearrangement.

Chapter 2

Materials and Methods

2.1 Chemicals

Solutions were made with chemicals purchased from Sigma-Aldrich (St. Louis, USA), Merck (Darmstadt, Germany) or VWR (Radnor, PA, USA) and dissolved in water purified with a MilliQ™ (Millipore, Bedford, USA) system. All solutions were filtered with 0.22 μm Millipore™ filter before usage.

2.2 Proteins

2.2.1 Actin Labeling and Polymerization

60 μl of Alexa Fluor® 488 Phalloidin or Alexa Fluor® 647 Phalloidin (Molecular Probes) were separated into 9 clean 1.5 ml Eppendorf tubes and dried in SpeedVac for approximately 30 min. The reddish pellet was then dissolved in 5 μl methanol and diluted with 85 μl labeling buffer (10 mM MOPS (pH 7.0), 0.1 mM EGTA, 3 mM NaN_3).

Meanwhile, a 39.6 μM actin solution (Actin/Actin-Biotin ratio of 5:1) was prepared by mixing rabbit skeletal actin monomers (32 μl , 2 mg/ml, Molecular Probes) with biotinylated rabbit actin monomers (1.6 μl , 10 mg/ml, tebu-bio/Cytoskeleton Inc., Denver, USA). The polymerization was initialized by adding 1 mM DTT, 1 mM ATP, 10 mM Tris-HCl (7.4), 2 mM MgCl_2 and 50 mM KCl in the

exact order specified to the actin mixture. The polymerization starts immediately after salt is added. A total volume of 48 μl was obtained and incubated at room temperature. After 1 hour of incubation time, 46 μl of labeling buffer was added to obtain a final actin concentration of 20 μM .

In order to stabilize the actin polymers, 10 μl were incubated with 90 μl of prepared Phalloidin solution for ~ 5 hours at RT and stored at 4 $^{\circ}\text{C}$.

2.2.2 Rabbit Muscle Myosin II Purification

Vertebrate smooth muscle myosin II was purified from rabbit muscle tissue according to ref. [20].

2.2.3 Dialysis of Myofilaments for Length Determination

20 μl of 15 μM Myosin II monomers were dialyzed (MWCO 12-14 kDA D-TubeTM Dialyzer Mini, Novagen) in ~ 25 ml equilibration buffer with various KCl concentrations (50/75/100/150/200 mM KCl, 2 mM MgCl_2 , 1 mM DTT, 10 mM Tris-HCl (pH 7.2)) for 1.5 days at 4 $^{\circ}\text{C}$. The equilibration buffer was exchanged 3 times after every ~ 6 hours and stirred by magnetic stirrer during the entire process. The myosin II solution was then diluted with corresponding equilibration buffer to 1 μM . As a final step, 5 μl of diluted myosin II was added to 500 μl equilibration buffer (20 μl in 480 μl for 150 and 200 mM KCl due to significant volume increase during dialysis) to transfer the probe onto the plasma-cleaned AFM cover slip.

2.3 Minimal Actin Cortex Assembly

Lipids were purchased from Avanti Polar Lipids, Inc. (Alabaster, AL). The lipid stock solutions should be warmed to RT before usage in order to prevent water condensation and subsequent volume increase. Mica plates were purchased from Shree GR exports PVT. LTD. (Kolkata, India).

A final lipid amount of 1 mg with 0.02% (mol/mol) DiD or 0.1% (mol/mol) di-4-ANEPPDHQ and either 1%, 0.1% or 0.01% (mol/mol) DSPE-PEG₂₀₀₀-Biotin

was used for all lipid mixtures. The mixture used for dynamical and domain deformation studies consisted of a 3:3:1 ratio of DOPC (1,2-dioleoyl-*sn*-glycero-3-phosphocholine), PSM (N-palmitoyl-D-*erythro*-sphingosylphosphorylcholine) and cholesterol with 0.1% (mol/mol) DSPE-PEG₂₀₀₀-Biotin. All lipids used within this study are found in many higher cell types and therefore strengthen the biological applicability of its results. Sphingomyelin for example is appreciated as partner for hydrogen bonding with the 3-OH group of cholesterol via its ester linkage. The intermolecular bonding is argued to promote lipid raft formation [22].

The solution was mixed within a 5 ml vial. The vial was then held almost horizontally and rotated during solvent evaporation under nitrogen flux in order to maximize the lipid pellet's surface. The vial was placed for another 15 min under nitrogen flux followed by vacuum for ~1 hour with aluminium foil covered to prevent bleaching the fluorescent dye. The lipids were rehydrated in 200 μ l SLB buffer (150 mM KCl, 25 mM Tris-HCl (pH 7.5)) by vigorous vortexing for several minutes. The solution of liposomes was then sonicated for approximately 30 minutes, divided into 10 aliquots (20 μ l/aliquot) and kept at -28 °C.

Cover glasses (22×22 mm, #1.5, Menzel Gläser, Thermo Fisher, Braunschweig, Germany) were intensively cleaned by sonication in Helmanex III (Hellma GmbH, Müllheim, Germany) for >1 h followed by 70% ethanol for another hour. Cover glasses were treated with MilliQ water and blow-dried before experiments were conducted. In order to use the assembled lipid bilayer with TIRF, one has to fixate freshly cleaved mica plates with immersion oil on the cover slide. A cut 1.2 ml Eppendorf tube was then glued with UV sensitive glue on the mica. Additional glue has to be placed from the outside at the boundary between glass and plastic due to a high temperature gradient during bilayer assembly (different expansion coefficients). The glue is hardened with 356 nm light for 20 min.

Meanwhile 20 μ l of frozen liposomes (5 mg/ml) were diluted in 130 μ l buffer A (50 mM KCl, 2 mM MgCl₂, 1 mM DTT and 10 mM Tris-HCl buffer (pH 7.5)) and sonicated until the solution turned clear (~30 min).

Both the self-assembled chamber and small unilamellar vesicles (SUV) solution were placed on heater (Dri-Block[®], Bibby Scientific Ltd., Staffordshire, UK) and slowly warmed above the demixing temperature (55 - 60 °C). 75 μl of SUVs were gently added on mica after the temperature was stable at the set-point and incubated for >45 min with 1 mM CaCl_2 in order to promote vesicle fusion. The lipid bilayer was washed with approximately 2 ml of warmed buffer A and gentle pipetting. The chamber with heating block was then removed from heating source and slowly cooled down to room temperature.

2 μl of unlabeled or Oregon-Green labeled NeutrAvidin[®] (1 mg/ml, Molecular Probes) were diluted in 200 μl buffer A and added to the supported lipid bilayer. The reaction buffer was washed after 10 minutes with >2 ml buffer A to remove unbound protein. 20 μl of 2 μM stabilized Alexa-488-phalloidin labeled biotinylated actin was then added and again incubated for >45 min at RT. The solution was gently washed with 400 μl buffer A to remove unbound actin polymers.

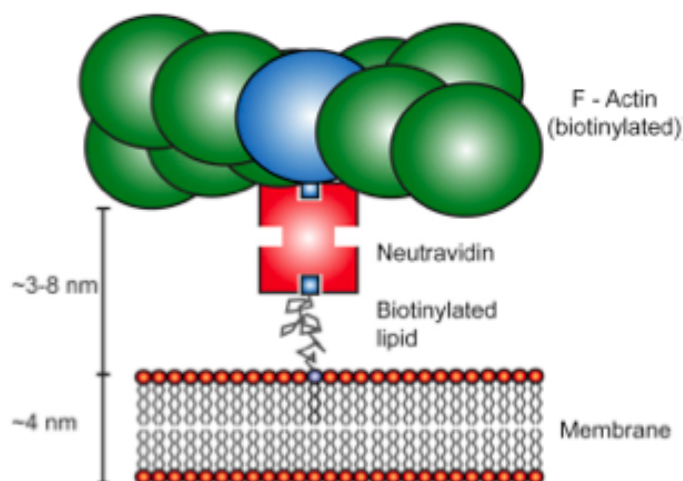


Figure 2.1: Illustration of assembled minimal actin cortex on lipid bilayer without support. The biotinylated actin filament is attached to the bilayer via the adaptor protein neutravidin and the biotinylated lipid DSPE-PEG₂₀₀₀-Biotin. Image adapted from ref. [9].

The sample was placed on the TIRF microscope and contraction was initialized with the addition of 200 μl of equilibrated myofilaments (4 μl Myosin II monomers, 0.5 mM ATP, 50 mM KCl, 2 mM MgCl_2 , 1 mM DTT and 10 mM Tris-HCl buffer (pH 7.5)) after first frames were acquired.

2.4 Microscopy

2.4.1 Atomic Force Microscopy

Atomic force microscopy was performed using a NanoWizard[®] AFM system (JPK Instruments, Berlin, Germany). The AFM head was mounted on top of a stable cast-iron microscope stage. Soft, rectangular silicon cantilevers (CSC38/noAl, Micromash, Tallin, Estonia) with a nominal spring constant of 0.03 N/m were used. The cantilever sensitivity in V/m was determined before each measurement.

Clean, circular glass cover slips ($d = 24$ mm, #1.5, Menzel Gläser, Thermo Fisher, Braunschweig, Germany) were hydrophilized by air plasma cleaning (MiniFlecto[®], plasma technology, HR, Germany). The assembled AFM fluid cell was filled with 500 μ l of protein solution. Residual non-adherent filaments were removed after 15 min by washing with equilibration buffer. AFM imaging was performed in contact mode with a scan rate of 1 Hz. The imaging forces were kept very low (<0.5 nN) by continuously adjusting the deflection setpoint and using optimized feedback gains. Raw AFM images were processed by using JPK Data Processing Software.

2.4.2 Total Internal Reflection Microscopy

TIRF microscopy was performed with components purchased from Zeiss (Axio Observer D1 Body and TIRF Slider), Cairo-Research (OptoSplit II Beam Splitter), Acal BFI (Laser Box) and assembled on a vibration-free optical table. A plan-apochromat Zeiss 100x/NA 1.46 objective and immersion oil with $n=1.518$ (23 °C) was used. The Andor iXon Ultra camera (Belfast, UK) with a resolution of 512x512 pixels and a pixel size of 16x16 μ m was used throughout all experiments (100 ms exposure time, 300 electron gain). Experiments were performed with 491 nm (50 mW Colbolt Calypso) and 640 nm (140 mW omikron LuxX 642-140) diode lasers. Emission spectra was collected and splitted using a beam splitter (AHF Analysentechnik AG, Tübingen, Germany) which reflects from 450 - 620 nm (≥ 90 %) and transmits from 645 - 900 nm (≥ 90 %).

Images were acquired with „Andor Solis for Imaging“ (Andor Solis, Belfast, UK) every 2.5 sec in interleaved mode using custom-written LabView software (National Instruments, Austin, TX). Laser intensity was optimized for every sample individually.

2.4.3 Laser Scanning Microscopy

FRAP experiments were conducted with a commercial LSM 510 Zeiss confocal microscope. A water-immersion LD C-Apochromat Zeiss 40x/1.1 W Korr UV-Vis-IR objective was used with 488 nm and 633 nm laser and 5.0% intensity. A beamsplitter HFT 488/633 and NFT 635 VIS was used in order to split emission spectrum. The emission was further filtered with LP 655 for DiD and BP 505-610 IR for Oregon-Green NeutrAvidin. Two APD sensors with optimized settings were used for image acquisition.

Image stacks were acquired after bleaching both dyes with 100% laser intensity (488 nm and 633 nm simultaneously) with an interval of 2 seconds for a total number of 25 frames. Data was processed with Zen 2009 software (Carl Zeiss, Jena, Germany).

2.5 Data Analysis

2.5.1 Software

Fiji software was used for analyzing and processing the acquired image series. Double color image stacks were aligned on beads (0.1 μm TetraSpeck™ microspheres, Invitrogen) with Fiji's plugin Descriptor-based series registration [7]. Matlab (The MathWorks Inc.) and Origin Pro 9.0.0G (OriginLab Corporation, Northampton, USA) were used for data analysis.

2.5.2 Analysis of di-4-ANEPPDHQ data

The emission spectrum of the fluorescent dye di-4-ANEPPDHQ is known to be different in liquid ordered and disordered phases of lipid membranes. In order to visualize possible lipid packing changes within phases during actomyosin contraction, image stacks acquired with TIRFM were processed with custom-written scripts using Fiji software. The generalized polarization (GP) value was calculated according to equation 2.1 adapted from ref. [14].

$$GP = \frac{I_{450-620nm} - I_{645-900nm}}{I_{450-620nm} + I_{645-900nm}} \quad (2.1)$$

Actomyosin activity was imaged by TIRFM in interleaved mode exciting 647-Phalloidin labeled F-actin with 640 nm and di-4-ANEPPDHQ with 488 nm. Signals were collected at 450-620 nm and 645-900 nm for di-4-ANEPPDHQ and at 645-900 nm for 647-Phalloidin labeled F-actin.

2.5.3 FRAP Analysis

In order to take the different physical properties within the liquid ordered and liquid disordered phases into account, we bleached areas predominantly occupied with the respective liquid state. The quantitative interpretation of FRAP curves is clearly limited due to the lack of an accurately defined system (domain shape, phase population). Nonetheless, insightful qualitative conclusions can be drawn for its dynamic behavior.

The intensity was averaged over the bleaching area and a area in the vicinity as reference. Data was normalized with equation 2.2 with the minimum at 0% recovery.

$$I_{norm} = \frac{I_{bleach} - I_{nonbleach}}{\max(I_{bleach} - I_{nonbleach}) - \min(I_{bleach} - I_{nonbleach})} \quad (2.2)$$

2.5.4 Simplified Active Contour Algorithm

The region of interest was isolated and automatically thresholded according to Otsu's algorithm implemented in the open-source software Fiji. The binary image stack was then read into a custom-written MATLAB script to record the deformation of liquid ordered phases. The area and boundary are obtained with the commands *regionprops* and *bwboundaries* for every frame in the image stack.

A simplified active contour or snake algorithm was further implemented in order to obtain the boundary displacement during actomyosin contraction. The initial boundary was therefore used as the reference contour and interpolated with the command *spline*. Contours are divided into a user-defined amount of points (snaxel points, $n=40$) with the command *linspace* and propagated to the boundary of the next frame along its normal vectors. The propagation was performed under specified conditions defined by

$$E = \frac{1}{2}(\alpha \left\| \frac{d\mathbf{v}}{ds}(\mathbf{s}) \right\|^2 + \beta \left\| \frac{d^2\mathbf{v}}{ds^2}(\mathbf{s}) \right\|^2). \quad (2.3)$$

The first term of equation 2.3 minimizes the distance between snaxel points during propagation and intuitively introduces a spring force between all contour points. The second term applies a force to every point in order to maintain a smooth curvature along the contour. Their individual weights are controlled by the user-defined coefficients α (0.002) and β (0.1). An existing algorithm was implemented to obtain the intrinsic snake properties [5].

The euclidean distance was calculated for every contour point and tracked from the initial to final boundary.

Chapter 3

Results

3.1 Minimal Actin Cortex Assembly on Phase Separated Membrane

A ternary lipid mixture of 3:3:1 cholesterol, 1,2-dioleoyl-*sn*-glycero-3-phosphocholine (DOPC) and N-palmitoyl-D-*erythro*-sphingosylphosphorylcholine (PSM) was assembled on solid support for this study in order to observe the behavior of a contractile minimal actin cortex on a liquid ordered and liquid disordered phase separated membrane [22].

Actin filaments are bound to the lipid membrane mimicking the complex actin cortex attached to the inner plasma membrane of all eukaryotic cells. The *in vitro* polymerization of actin is performed with a ratio of 5:1 monomeric actin and monomeric biotinylated actin. Partially biotinylated actin filaments are attached via neutravidin to biotinylated lipids incorporated into the phase separated lipid membrane¹. The density of the minimal actin cortex is directly controlled by changing the concentration of biotinylated lipids, which subsequently reduces or increases the actin binding sites at the membrane. In order to obtain a medium dense actin cortex, DSPE-PEG₂₀₀₀-Biotin was added to the lipid mixture at a 0.1% (mol/mol) concentration.

¹The avidin-derived protein neutravidin is uniquely suited as an adaptor because of its superior affinity for biotin ($K_d = 10^{-15}$ M, 4 biotin-binding sites)

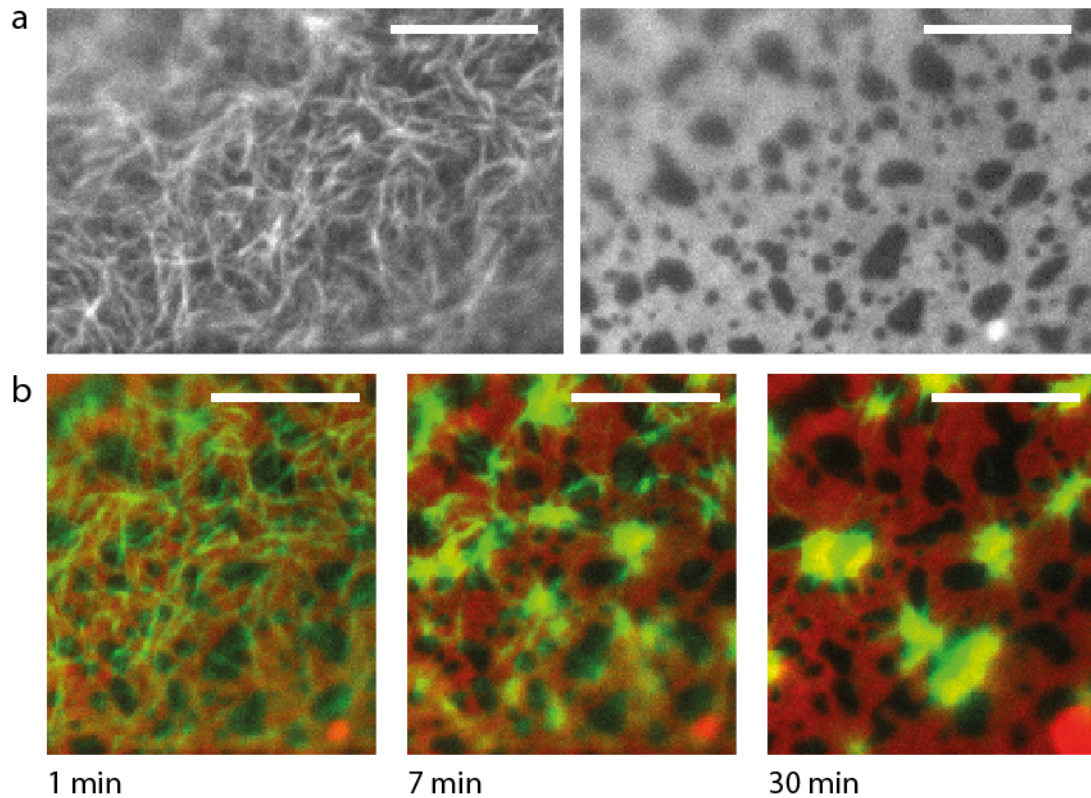


Figure 3.1: b) Contraction of medium dense actin cortex on a phase separated membrane (3:3:1 DOPC:PSM:Cholesterol, 0.1% DSPE-PEG₂₀₀₀-Biotin) was induced by the addition of myofilaments and 0.5 mM ATP. Observed by TIRFM with a) Alexa-488 Phalloidin labeled actin filaments (left) and 0.02% DiD labeled membrane (right). Scale bar, 10 μm .

Contraction of the minimal actin cortex is induced by the addition of 0.5 mM ATP and myofilaments with a characteristic length of 500-600 nm, which equals 30 interacting myosin heads per myofilament in average [23]. The medium dense actin cortex bound to the phase separated membrane is shown before and after induction in figure 3.1. Actin filaments were evenly distributed over liquid ordered and disordered phases whereas DiD was located exclusively in liquid disordered phases (figure 3.1 a). Similar contraction rates in comparison with the original actomyosin study, which used Egg PC for lipid bilayer formation [23], were obtained. The contraction of filamentous actin was observed to lead to the formation of aster-like complexes at the boundary of liquid ordered and disordered phases within the time range of minutes (figure 3.1 b).

Theoretical studies concerned about the dynamic behavior of myofilaments on

F-actin showed that the mean fraction of myosin heads attached to actin during one reaction cycle (duty ratio) is inversely proportional to the concentration of ATP, which means that the processivity of myofilaments at high ATP is less [23]. The contractile speed can therefore be regulated by the concentration of ATP as one of a myriad of possible parameters.

3.2 Length Distribution of Equilibrated Myofilaments

In order to titrate the locomotive activity of myofilaments with ATP in a future study, we determined the characteristic length distribution of myofilaments at different KCl concentrations. We used atomic force microscopy in order to characterize the length distribution alias myosin heads per filament.

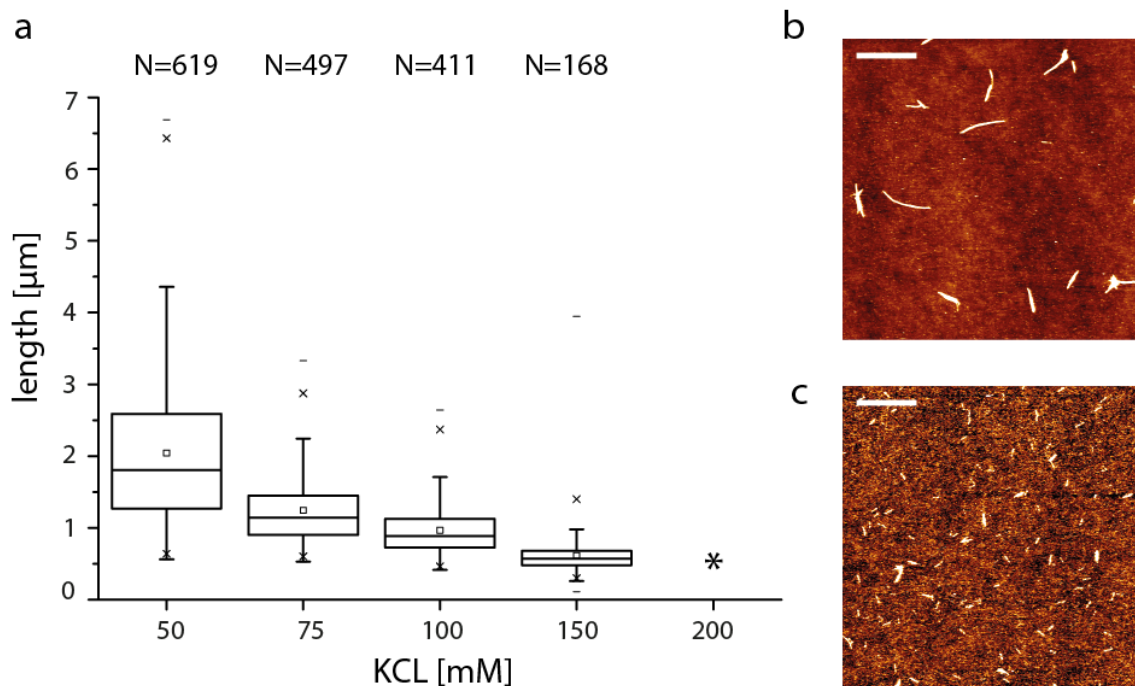


Figure 3.2: a) Length distribution of myofilaments which were equilibrated in various KCl concentrations and measured with atomic force microscopy. Images of myofilaments at (b) 50 mM KCl and (c) 150 mM KCl. (*) Filaments at 200 mM KCl were not sufficient resolvable for length determination. Scale bar, 5 μm

As the concentration of potassium chloride increases, the median length and distribution spread decreases in a non-linear fashion. Median length values of

$1.81 \pm 1.15 \mu\text{m}$ for 50 mM KCl, $1.14 \pm 0.47 \mu\text{m}$ for 75 mM KCl, $0.88 \pm 0.35 \mu\text{m}$ for 100 mM KCl and $0.57 \pm 0.25 \mu\text{m}$ for 150 mM KCl were obtained. Length determination at 200 mM KCl could not be conducted because the smaller and more fragile myofilaments were either destroyed or not sufficient resolved during AFM imaging.

It is important to note that different water influx rates across the semipermeable membrane during equilibration have to be taken into account for further analysis. The osmotic pressure leads to a significant volume increase at higher salt concentrations which effects the myosin concentration and presumably the accumulation to myofilaments. Knowing the plain length distribution was however sufficient for our purposes.

3.3 Dynamic Behavior of the Biotinylated Lipid DSPE

The biotinylated lipid DSPE as actin's connection to the lipid bilayer, pose the critical element for actin cortex and membrane interactions. We investigated for that reason the diffusion behavior of the biotinylated lipid DSPE on the phase separated membrane consisting of 3:3:1 DOPC:PSM:Cholesterol and 0.02% (mol/mol) DiD by FRAP experiments. Biotinylated lipids were added to the lipid mixture at a 0.1% (mol/mol) concentration and labeled with Oregon-Green neutravidin.

As seen in figure 3.3 b), the hydrophobic membrane dye DiD recovers with the same speed for both phases. Membrane defects are therefore excluded across FRAP experiments. Figure 3.3 a) shows the difference of DSPE-PEG₂₀₀₀-Biotin-Neutravidin recovery in L_o and L_d phase. The diffusion into liquid ordered phases was observed to be much slower than the recovery rate in liquid disordered phases. The recovery rate was however superimposed by the diffusion behavior in both phases because of the circular bleaching area exceeding the actual L_o domain in the membrane. We further believe that the steady-state for L_o domain recovery was not reached after a time of 180 sec which would indicate a initial diffusion to the phase boundary and a much slower hopping rate across the boundary. The dynamic behavior of the biotinylated lipid could therefore be described by at least

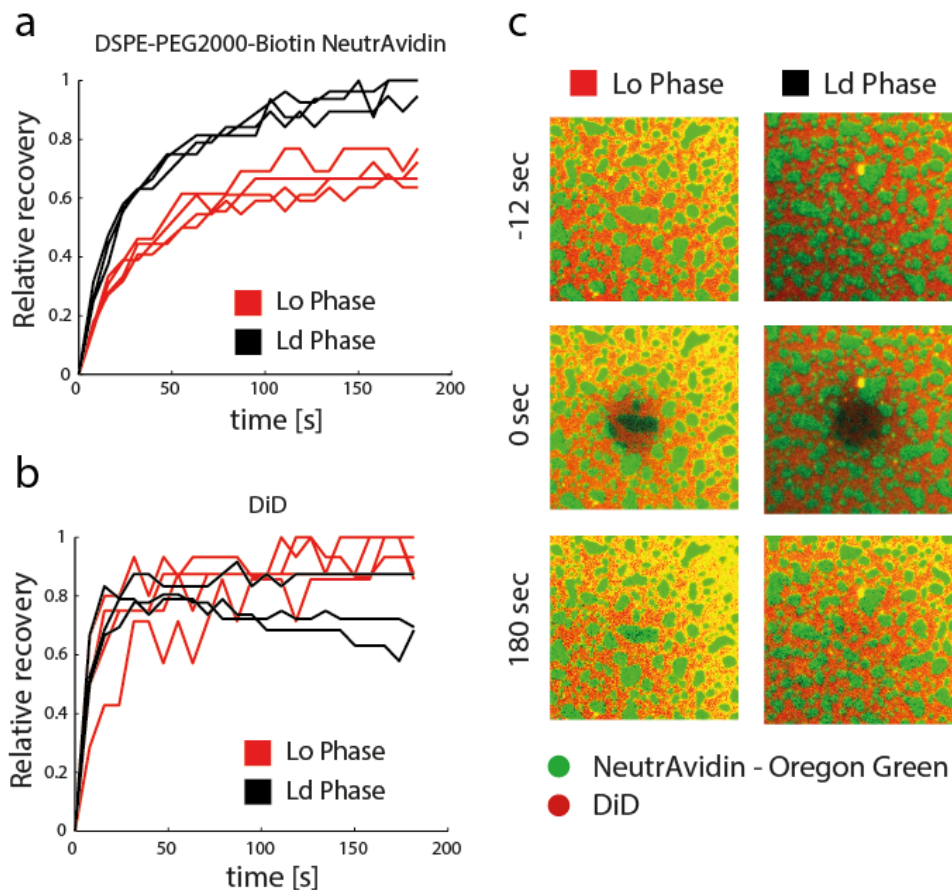


Figure 3.3: Fluorescence recovery after photobleaching analysis was performed on a 3:3:1 DOPC:PSM:Cholesterol membrane with 0.1% (mol/mol) biotinylated lipid. The bleaching area was chosen by following criteria: large L_o domain for FRAP in L_o phases (c-left column) and sparsely populated with small L_o domains for FRAP in L_d phases (c-right column). Normalized intensity curves of (a) the lipid anchor DSPE-PEG₂₀₀₀-Biotin with neutravidin and (b) the hydrophobic membrane dye DiD are showing the relative recovery over time in liquid ordered (■) and liquid disordered (■) phases.

three kinetic components, one being the diffusion of DSPE in the liquid disordered phase, the second one being the slow hopping rate between L_d and L_o phase and the third one being the diffusion rate within the liquid ordered domain.

3.4 Deformation of Phase Boundaries by the Contractile Actomyosin Network

Knowing the dynamic behavior of Oregon-Green labeled anchor lipids qualitatively from FRAP experiments, we then studied the contractile behavior of Alexa-488 Phalloidin labeled F-actin on phase separated membranes (0.1% DSPE-PEG₂₀₀₀-Biotin, 3:3:1 DOPC:PSM:Cholesterol, 0.02% DiD) with TIRFM. Due to the difference in motion of slow hopping biotinylated lipids and the faster actomyosin contraction, we believed that both, the contractile behavior of actomyosin as well as the lipid phases, are influenced by each other at phase boundaries.

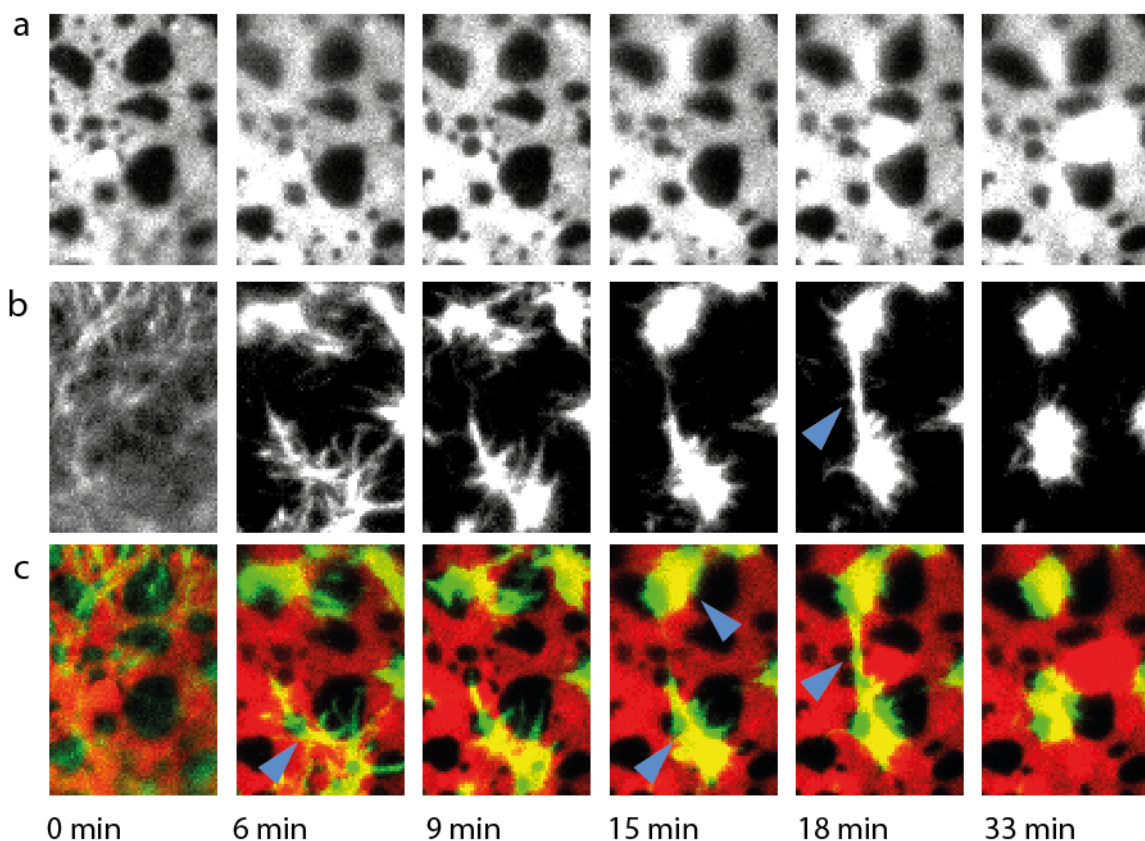


Figure 3.4: a) DiD labeled 3:3:1 DOPC:PSM:Cholesterol membrane, b) Alexa-488 Phalloidin labeled actin filaments, c) Composed images of a) and b). Image sequence of contracting F-actin asters via actin bond (arrowhead in b and c at 18 min). Asters were forming at the interface of liquid ordered and disordered phases (arrowhead in c at 6 min) which constrained their movement along the boundary (arrowhead in c at 15 min).

As seen in figure 3.4, F-actin polymers accumulated at the boundary of liquid ordered and disordered phases during actomyosin contraction. F-actin asters were further contracted by myosin motors via the connection indicated by the arrowhead in 3.4 b) at 18 min. Actin polymer displacement appeared to be constrained by phase boundaries as indicated by the arrowheads at 15 min. The hindered movement of F-actin bound to the biotinylated lipid further suggested a slower hopping rate of DSPE over the boundary of L_o and L_d phases. This finding consists with what we observed with FRAP experiments.

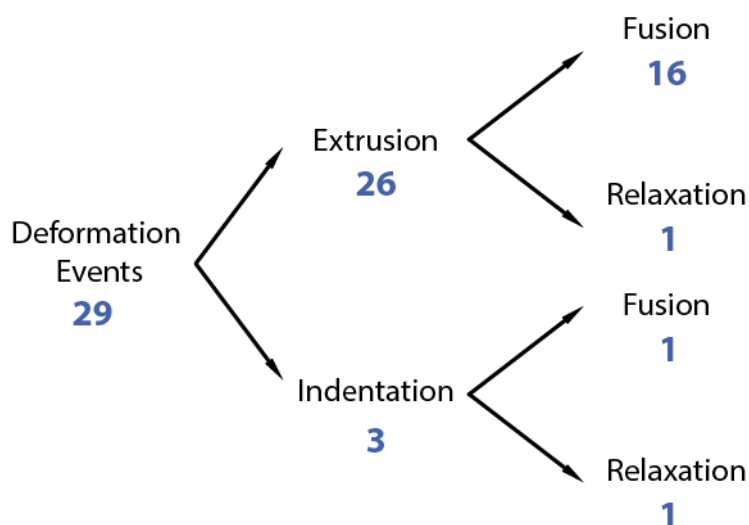


Figure 3.5: Probability tree of observed deformation events during actomyosin contraction on phase separated membrane. A total number of 29 deformation events were counted which were divided into two subsets, named extrusion (deformation direction from liquid ordered into disordered phases) and indentation (liquid ordered domains were pushed in by contractile actomyosin network). Subsequent events were further categorized into fusion (with other liquid ordered domains) and relaxation events (relaxation of deformed phase boundary to initial position). Extrusion events were observed frequently with a occurrence rate of 90% of all deformation events. If liquid ordered domains were located in the vicinity of deformation events, the extrusion eventually led to fusion events (61 %).

While imaging the actomyosin contraction on membranes, we observed in few cases bright balloon-like shapes emerging from the membrane and pushing F-actin during growth. The 3-dimensional structure had however minor effects on actomyosin contraction and phase deformation.

The probability tree shown in figure 3.5 visualizes the rate and order of occurrence of deformation events observed during actomyosin contraction on the phase separated membrane. Deformation events were divided into extrusion (liquid ordered phases were pulled out) and indentation (liquid ordered phases were pushed in) which were further subdivided into fusion with other liquid ordered phases and relaxation events. 90% of deformation events led to the extrusion of liquid ordered domains. In the case that L_o domains were present in the vicinity of deformation events, 61% of extrusion events resulted in fusion events. Indentation events were on the other hand rarely observed (10% of all deformation events).

The relaxation of displaced boundaries to their initial position appeared to be initialized after F-actin dissociated from the boundary. But only few cases were observed as seen in figure 3.5.

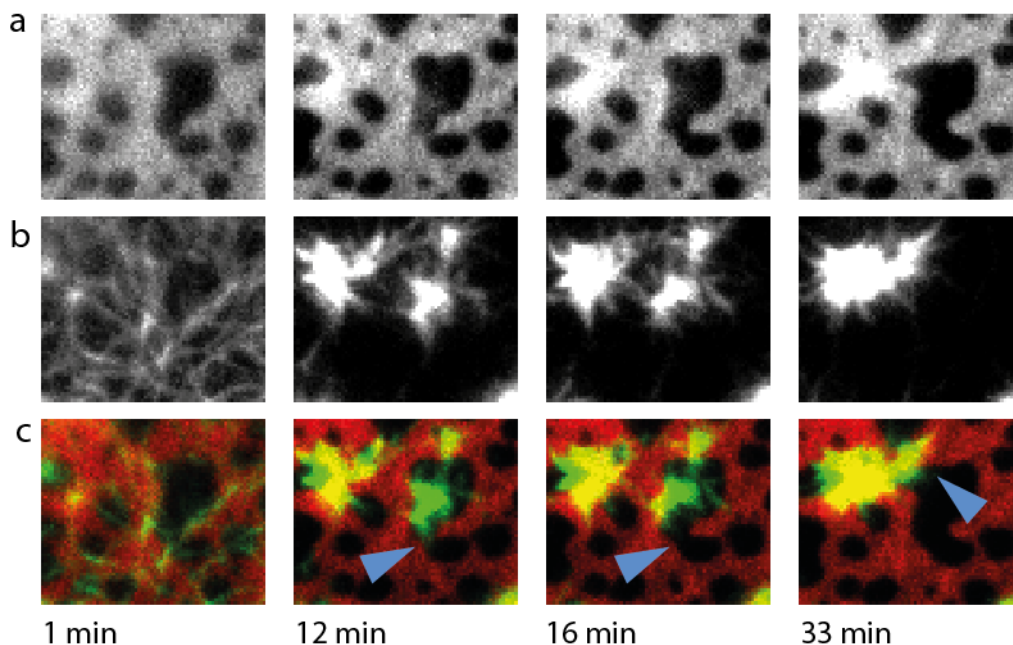


Figure 3.6: Example for extrusion event for liquid ordered phases. Image sequence of a contractile b) Alexa-488 Phalloidin labeled actin cortex on a) DiD labeled phase separated membrane; c) Composed images of a) and b). Aster was pulled by upper aster over the L_o phase which resulted in fusion (lower arrowhead at 12 and 16 min) and extrusion (upper arrowhead at 33 min) of boundary.

One example for the frequently observed extrusion and subsequent fusion events is shown in figure 3.6. The large aster was pulling accumulated F-actin over a liquid disordered phase bridging two liquid ordered domains at 16 min by the initial extrusion. The upper domain was further extruded at 33 min (blue arrow). Extrusion of liquid ordered domains led to a increase in area and vanishing of smaller L_o domains in the closer vicinity during boundary deformation. It is however difficult to assign this vanishing effect to thermal fluctuations while imaging or to fusion events.

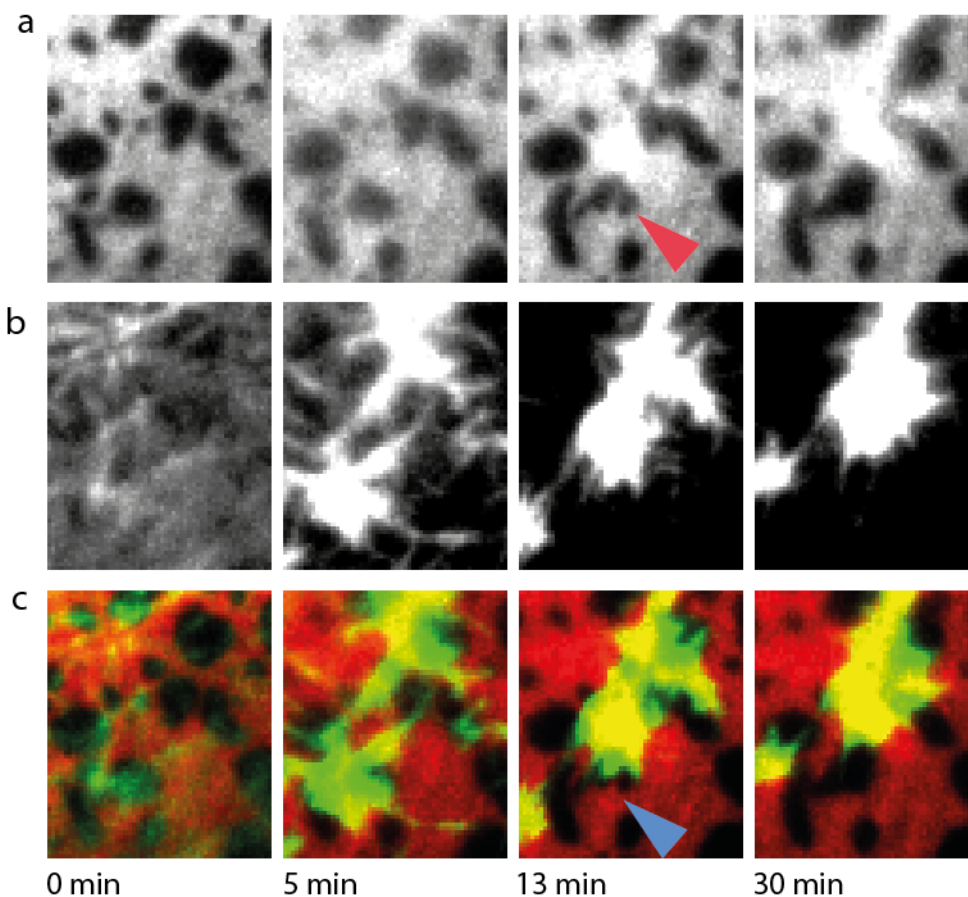


Figure 3.7: Example for indentation events of liquid ordered phases. The attraction of two actin asters bound to a) DiD labeled phase separated membrane led to the indentation of a L_o domain (red arrowhead in column a at 13 min); b) Alexa-488 Phalloidin labeled actin filaments, c) Composed images of a) and b). Stabilized large aster pulled lower F-actin aster across the concave profile of smaller domain. The phase boundary relaxed back to the initial position shortly after actin filaments passed the lower phase boundary.

Furthermore, figure 3.7 illustrates one example for the less often observed domain indentation (10% of all noted deformation events) from L_d to L_o phases. The lower actin pole was pulled across the convex profile of a L_o phase leading to the indentation at 13 min (red arrowhead). The domain relaxed back to its initial position shortly after F-actin dissociated from the boundary.

Deformed phase boundaries with a higher curvature and boundary length appeared to relax back to their initial properties shortly after F-actin dissociated from the phase boundary. Minimizing the boundary length between different phases indicates dynamic rearrangement of lipids due to line tension [8]. As seen in figure 3.8, three liquid-ordered domains were fused and extruded during <12 minutes. The smaller domain (blue arrow) relaxed back at 24 minutes in order to minimize boundary length. The dynamic adaptation to changes in the system further excluded the possible disintegration of lipid bilayers during actomyosin contraction.

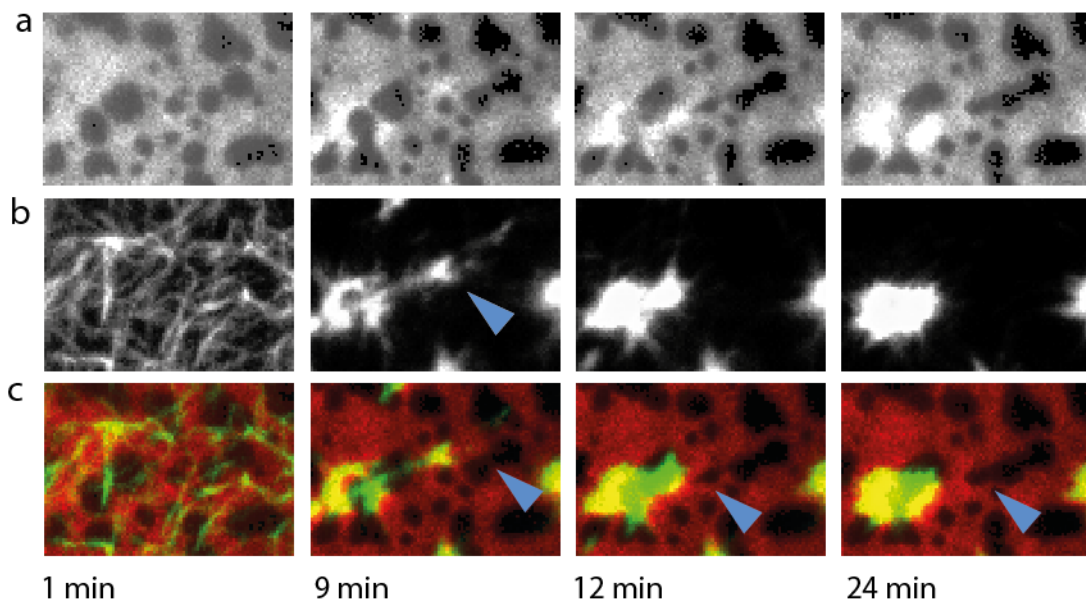


Figure 3.8: Sequential b) Alexa-488 Phalloidin labeled actin cortex contraction by myofilaments on a) DiD labeled phase separated membrane; c) Composed images of a) and b). Small aster (arrowhead in column b at 9 min) was pulled by aster (lower left corner) across three domains which fuse (9,12 min), deform (12 min) and relax (24 min) in order to minimize the boundary length due to line tension.

It is important to note that membranes, which had minor defects most likely originated from the assembly process, were disintegrated during actomyosin contraction after several hours. Scavengers were able to minimize phototoxic reactions repressing the disintegration of membranes. Disintegration of membranes started at membrane defects (holes) and spread over the entire field of view radial symmetrically. The deformation of phases due to actomyosin contraction was however highly asymmetric and concentrated at phase boundaries which suggests that disintegration and deformation are easily distinguished.

3.5 Quantitative Analysis of Phase Deformation

The quantification of phase deformation was performed with the proposed simplified active contour algorithm and the fluorescent dye di-4-ANEPPDHQ.

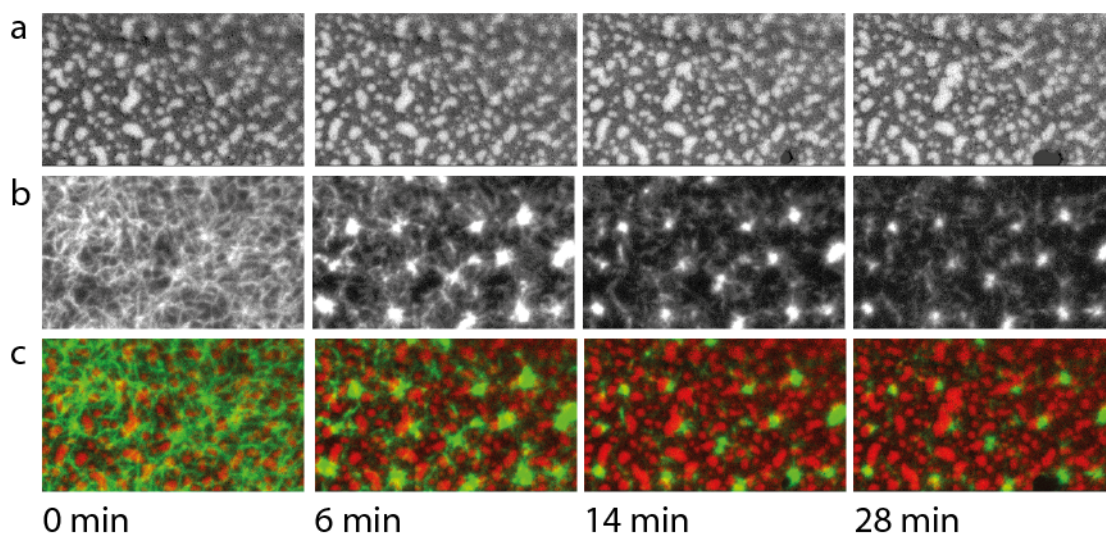


Figure 3.9: Contraction of medium dense 647-Phalloidin labeled actin cortex (b) by myofilaments on 0.1% (mol/mol) di-4-ANEPPDHQ labeled 3:3:1 DOPC:PSM:Cholesterol membrane. Images were acquired in interleaved mode exciting di-4-ANEPPDHQ with 488 nm laser (collecting signals from 450-620 nm and 645-900 nm) and 647-Phalloidin labeled F-actin with 640 nm. GP value of di-4-ANEPPDHQ signal (a) was calculated according to ref. [14]. c) Composed image sequence of both channels.

Di-4-ANEPPDHQ, which is described to be a specific probe for lipid packing order [14], is known to emit at approximately 560 nm for ordered phases and

with a broad distribution around 620 nm for liquid disordered membrane phases. The generalized polarization (GP) value, the emission ratio between the range of 450-620 nm and 645-900 nm, was obtained according to ref. [14]. Generalized polarization values are shown in figure 3.9 a) ranging from -1 (black, liquid disordered) to +1 (white, liquid ordered).

Analyzing the GP value during actomyosin contraction with the solvatochromic fluorescent dye di-4-ANEPPDHQ showed no conclusive results for a lipid packing change within phases. The emission signal was however not optimized due to missing filter sets for the TIRF setup.

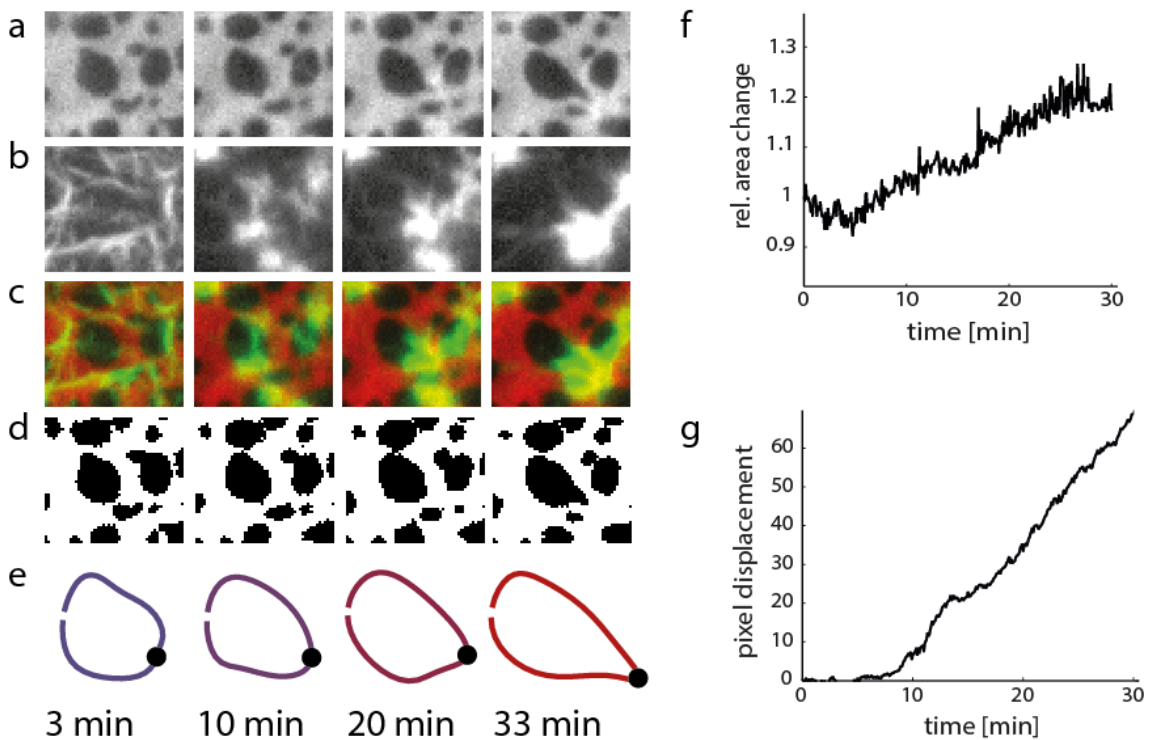


Figure 3.10: Proposed simplified active contour algorithm was applied to L_0 phase deformations. After automatically thresholding the image sequence of 488-Phalloidin labeled actin (b) on DiD labeled 3:3:1 DOPC:PSM:Cholesterol membrane (b) according to Otsu's method (d), the active contour algorithm was applied to the binary image stack (e). Liquid ordered domain area growth and maximal snaxel point displacement as indicated by the black dot in e) were tracked over time and plotted in f) and g). Local plateau in g) of snaxel point displacement at approximately 14 min correlates with temporally non-moving actomyosin.

The simplified active contour algorithm was used for the quantification of deformation events at liquid ordered phases. The contour points were divided by a discrete set of anchor points (snaxel points) in order to maintain a smooth curvature during the boundary propagation in subpixel space. Outward propagation was handled as positive displacement and inward propagation as negative.

As seen in figure 3.10, domain deformation by actomyosin contraction led to a relative area increase of around 20% obtained by MATLAB's built-in commands *regionprops* and *bwboundaries*. The maximum contour displacement is shown in 3.10 g) and highlighted by the black dot in e). The local plateaus, which indicate no boundary displacement, correlate with temporally non-moving actomyosin. The smaller kinks in pixel displacement (g) are difficult to interpret because of Outs's thresholding method and the interpolation mechanism applied during the active contour algorithm. It is tempting to interpret that actin filaments with a biotinylated ratio of 5:1 exhibit a discrete dragging of single or clustered DSPE lipids over the phase boundary by actomyosin resulting in a step-like acceleration of boundary displacement.

Since F-actin asters and domains were interacting during the entire image sequence, no relaxation could be analyzed with the proposed algorithm. Due to resolution limitations of TIRF microscopy, we were also not able to discriminate single actin filaments if bundled during contraction. Correlating the motion of actomyosin filaments during domain deformation with the total contour's pixel displacement on a molecular level was for that reason not possible.

Chapter 4

Conclusion and Future Prospects

4.1 Length Distribution of Equilibrated Myofilaments

The length distribution of myofilaments was shown to decrease with a higher concentration of KCl in a non-linear fashion by AFM imaging. It is important to note that the length deviation is higher for low concentrations of KCl which should be considered for the titration of actomyosin activity with ATP.

4.2 Contractile Behavior of Actomyosin on Phase Separated Membranes

We were able to observe a slow hopping rate of DSPE across the boundary of liquid ordered and disordered phases with FRAP experiments. The faster mobility of a rearranging actin cortex bound to the membrane by the biotinylated Lipid DSPE was therefore assumed to excite force to the boundary of the macroscopic lipid phases as we were able to observe with TIRFM eventually.

4.2.1 Mechanistic Observations at the Phase Boundary

Aster formation at the phase boundary might be explained by the hindered diffusion of actin filaments crossing the boundary. Freely diffusing F-actin without boundary affiliation are dragged towards the hindered F-actin by ATP-hydrolyzing myofilaments leading to the accumulation at boundaries as net result. If, on the

other hand, both F-actin asters are hindered by phase boundaries, the contraction leads to deformation events (see figure 4.1, upper image). The spatial distribution of F-actin poles depends therefore highly on the association to phase boundaries. The mean length of actin filaments and the average interspace between domains are certainly the most meaningful parameters for this model. Controlling these parameters is very difficult and may be pursued in a future study.

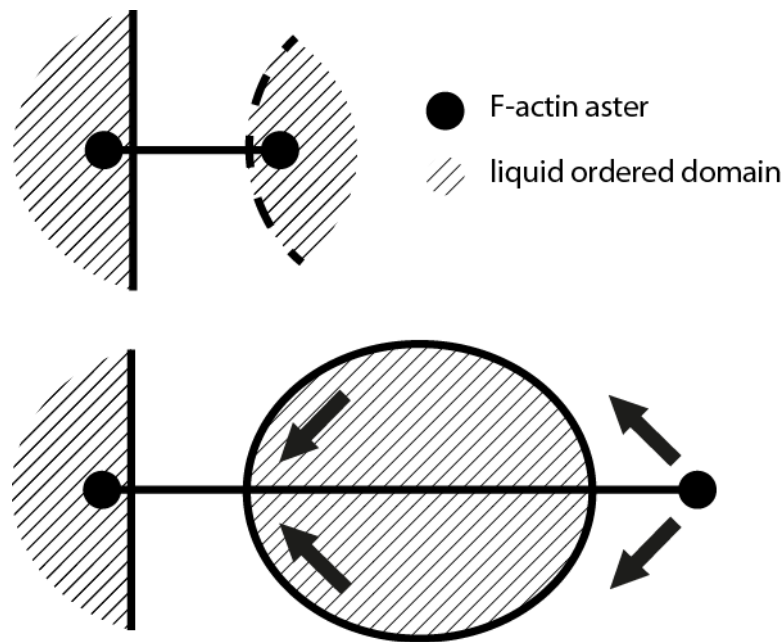


Figure 4.1: Schematic illustration of actomyosin contraction on phase separated membrane. Small F-actin asters forming at the boundary of liquid ordered and disordered phases. In case of hindered F-actin aster is connected to freely diffusing aster, the contraction leads to further accumulation at the phase boundary. If on the other hand both asters are associated with phase boundaries, the contraction results in phase deformation. Aster displacement was observed to be constrained by the boundary. Unlike concave profiles (left profile of liquid ordered domain), convex phase profiles disperse actomyosin activity along the phase boundary and reduces the path energy as indicated by arrows on the right side of illustrated L_o domain.

Liquid ordered phase indentation was observed rarely (10% of all deformation events) in comparison to extrusion events (90% of all deformation events). The motion of asters towards convex profiles might lead to the dispersion of force or

to the redirection of actin movement along the boundary minimizing the path energy. Concave shapes however concentrate force at the boundary and constrain F-actin movement leading to the accumulation of actomyosin activity at domain poles (see figure 4.1, lower image). We therefore concluded that the asymmetric deformation occurrence rate is rather explained by the domains geometrical shape and not by a asymmetric hopping rate of the biotinylated lipid across the boundary of liquid disordered and liquid ordered phases.

If additional domains were present in the closer vicinity, the boundary deformation eventually led to the fusion of liquid ordered phases as observed for 61% of all extrusion events. Indented or extruded domain boundaries appeared to minimize their boundary length after F-actin dissociation due to line tension. It was however only observed twice after deformation events. The displacement of F-actin asters appeared to be less than the distance that is needed to deform the phase boundary and dissociate on a regular basis.

4.2.2 Models for Area Growth of Phases

We believe that the area increase of liquid ordered domains by actomyosin deformation can be explained by at least two mechanism. The change of area per lipid by the transition from the liquid ordered to liquid disordered state would describe a certain increase in area. Opposing the transition is the increase in energy that would result if lipids change their packing state within the liquid ordered phase. The magnitude of approximately 70% as we observed for one case is therefore hardly explained by the phase transition exclusively.

The influx of lipids from the vicinity may therefore explain further area growth. Membrane deformation introduces a non-equilibrium state in the membrane, increasing the affinity for lipids which are able to counterbalance the intrusion. We were able to observe small domains vanishing in the closer vicinity during deformation which may be explained by the fusion of domains compensating high-energy lipid ordering transitions.

4.3 Biological Implications & Future Investigations

The rearranging actin cortex by motor proteins describes a new approach for membrane organization. Clustering of rafts might be induced not only by hydrogen bonding via sphingomyelin or protein crosslinking [11], but also by the directed displacement of raft proteins attached to dynamic F-actin polymers. Active reorganization of membrane proteins might further lead to a constant spatial and temporal synchronization of lipid/protein rafts and actin cortex remodeling.

In order to approximate minimal system closer to the biological cell, the friction coupling of lipids as observed in supported lipid membranes has to be avoided [15]. Future experiments should therefore consider free-standing membranes, e.g. giant unilamellar vesicles for the assembly of a minimal actin cortex on phase separated membranes. Unlike the focused deformation of phase boundaries in supported phase separated membranes, the boundary of lipid phases in free-standing membranes might promote the displacement of entire domains leading to the accumulation of phases at the aster formation site.

Bibliography

- [1] <http://gopubmed.org>. April 2013
- [2] ALLEN, John A. ; HALVERSON-TAMBOLI, Robyn A. ; RASENICK, Mark M.: Lipid raft microdomains and neurotransmitter signalling. In: *Nature Reviews Neuroscience* 8 (2006), Nr. 2, S. 128–140
- [3] BAUMGART, Tobias ; HESS, Samuel T. ; WEBB, Watt W.: Imaging coexisting fluid domains in biomembrane models coupling curvature and line tension. In: *Nature* 425 (2003), Nr. 6960, S. 821–824
- [4] BEAUSANG, John F. ; SHRODER, Deborah Y. ; NELSON, Philip C. ; GOLDMAN, Yale E.: Tilting and Wobble of Myosin V by High-Speed Single-Molecule Polarized Fluorescence Microscopy. In: *Biophysical journal* 104 (2013), Nr. 6, S. 1263–1273
- [5] DIRK-JAN KROON: *Active contour algorithm*. <http://www.mathworks.com/matlabcentral/fileexchange/28149-snake-active-contour>.
Version: Juli 2010
- [6] EHRIG, Jens ; PETROV, Eugene P. ; SCHWILLE, Petra: Near-critical fluctuations and cytoskeleton-assisted phase separation lead to subdiffusion in cell membranes. In: *Biophysical journal* 100 (2011), Nr. 1, S. 80–89
- [7] FERNANDEZ, Anita G. ; MIS, Emily K. ; BARGMANN, Bastiaan O R. ; BIRNBAUM, Kenneth D. ; PIANO, Fabio: Automated sorting of live *C. elegans* using laFACS. In: *Nature Methods* 7 (2010), Nr. 6, 417–418. <http://dx.doi.org/10.1038/nmeth.f.304>. – DOI 10.1038/nmeth.f.304. – ISSN 1548–7091, 1548–7105

- [8] GARCIA-SAEZ, A. J. ; CHIANTIA, S. ; SCHWILLE, P.: Effect of Line Tension on the Lateral Organization of Lipid Membranes. In: *Journal of Biological Chemistry* 282 (2007), September, Nr. 46, 33537–33544. <http://dx.doi.org/10.1074/jbc.M706162200>. – DOI 10.1074/jbc.M706162200. – ISSN 0021–9258, 1083–351X
- [9] HEINEMANN, Fabian ; VOGEL, Sven K. ; SCHWILLE, Petra: Lateral Membrane Diffusion Modulated by a Minimal Actin Cortex. In: *Biophysical journal* 104 (2013), Nr. 7, S. 1465–1475
- [10] JEAN-MARC ALLAIN ; (SECOND) MARTINE BEN AMAR: Budding and Fission of a multiphase vesicle. In: *arXiv:physics* (2008)
- [11] KUSUMI, Akihiro ; KOYAMA-HONDA, Ikuko ; SUZUKI, Kenichi: Molecular dynamics and interactions for creation of stimulation-induced stabilized rafts from small unstable steady-state rafts. In: *Traffic* 5 (2004), Nr. 4, S. 213–230
- [12] LIU, Allen P. ; FLETCHER, Daniel A.: Actin polymerization serves as a membrane domain switch in model lipid bilayers. In: *Biophysical journal* 91 (2006), Nr. 11, S. 4064–4070
- [13] MUNRO, Sean: Lipid rafts: elusive or illusive? In: *Cell* 115 (2003), Nr. 4, 377–388. <http://www.sciencedirect.com/science/article/pii/S0092867403008821>
- [14] OWEN, Dylan M. ; RENTERO, Carles ; MAGENAU, Astrid ; ABU-SINIYEH, Ahmed ; GAUS, Katharina: Quantitative imaging of membrane lipid order in cells and organisms. In: *Nature Protocols* 7 (2011), Dezember, Nr. 1, 24–35. <http://dx.doi.org/10.1038/nprot.2011.419>. – DOI 10.1038/nprot.2011.419. – ISSN 1754–2189, 1750–2799
- [15] PRZYBYLO, Magdalena ; SÝKORA, Jan ; HUMPOLÍČKOVÁ, Jana ; BENDA, Aleš ; ZAN, Anna ; HOF, Martin: Lipid Diffusion in Giant Unilamellar Vesicles Is More than 2 Times Faster than in Supported Phospholipid Bilayers under Identical Conditions. In: *Langmuir* 22 (2006), Oktober, Nr. 22, 9096–

9099. <http://dx.doi.org/10.1021/la061934p>. – DOI 10.1021/la061934p.
– ISSN 0743–7463, 1520–5827
- [16] RAJAGOPALAN, Srividya ; WACHTLER, Volker ; BALASUBRAMANIAN, Mohan: Cytokinesis in fission yeast: a story of rings, rafts and walls. In: *Trends in Genetics* 19 (2003), Juli, Nr. 7, 403–408. [http://dx.doi.org/10.1016/S0168-9525\(03\)00149-5](http://dx.doi.org/10.1016/S0168-9525(03)00149-5). – DOI 10.1016/S0168-9525(03)00149-5. – ISSN 01689525
- [17] SALBREUX, Guillaume ; CHARRAS, Guillaume ; PALUCH, Ewa: Actin cortex mechanics and cellular morphogenesis. In: *Trends in Cell Biology* 22 (2012), Oktober, Nr. 10, 536–545. <http://dx.doi.org/10.1016/j.tcb.2012.07.001>. – DOI 10.1016/j.tcb.2012.07.001. – ISSN 09628924
- [18] SELLERS, James R. ; KACHAR, Bechara: Polarity and Velocity of Sliding Filaments: Control of Direction by Actin and of Speed by Myosin. In: *Science Reports* 249 (1990), S. 406–408
- [19] SIMONS, K. ; SAMPAIO, J. L.: Membrane Organization and Lipid Rafts. In: *Cold Spring Harbor Perspectives in Biology* 3 (2011), Mai, Nr. 10, a004697–a004697. <http://dx.doi.org/10.1101/cshperspect.a004697>. – DOI 10.1101/cshperspect.a004697. – ISSN 1943–0264
- [20] SMITH, D. ; ZIEBERT, F. ; HUMPHREY, D. ; DUGGAN, C. ; STEINBECK, M. ; ZIMMERMANN, W. ; KAES, J.: Molecular Motor-Induced Instabilities and Cross Linkers Determine Biopolymer Organization. In: *Biophysical Journal* 93 (2007), Dezember, Nr. 12, 4445–4452. <http://dx.doi.org/10.1529/biophysj.106.095919>. – DOI 10.1529/biophysj.106.095919. – ISSN 00063495
- [21] STOSSEL, Thomas P. ; CONDEELIS, John ; COOLEY, Lynn ; HARTWIG, John H. ; NOEGEL, Angelika ; SCHLEICHER, Michael ; SHAPIRO, Sandor S.: Filamins as integrators of cell mechanics and signalling. In: *Nature Reviews Molecular Cell Biology* 2 (2001), Nr. 2, 138–145. http://www.nature.com/nrm/journal/v2/n2/abs/nrm0201_138a.html

- [22] VEATCH, Sarah ; KELLER, Sarah: Miscibility Phase Diagrams of Giant Vesicles Containing Sphingomyelin. In: *Physical Review Letters* 94 (2005), April, Nr. 14. <http://dx.doi.org/10.1103/PhysRevLett.94.148101>. – DOI 10.1103/PhysRevLett.94.148101. – ISSN 0031–9007, 1079–7114
- [23] VOGEL, Sven K. ; PETRASEK, Zdenek ; HEINEMANN, Fabian ; SCHWILLE, Petra: Myosin motors fragment and compact membrane-bound actin filaments. In: *eLife Sciences* 2 (2013)
- [24] WALKER, Matthew L. ; STAN A. BURGESS, (second) ; JAMES R. SELLERS, (third) ; FEI WANG, (fourth) ; JOHN A. HAMMER III, (fifth) ; JOHN TRINICK, (sixth) ; PETER J. KNIGHT, (seventh): Two-headed binding of a processive myosin to F-actin. In: *Nature Letters* 405 (2000), S. 804–807

Danksagung

Der Erfolg meiner Abschlussarbeit am Max-Planck-Institut in Martinsried, München wurde erst durch eine Vielzahl von hilfsbereiten Wissenschaftlern ermöglicht, denen ich bei dieser Gelegenheit danken will.

Zum einen möchte ich Prof. Petra Schwille für die motivierende Betreuung danken. Natürlich bedanke ich mich bei meinen direkten Betreuern Sven Vogel und Fabian Heinemann. Ohne dem erst kürzlich von Sven entwickelten Minimal-system wäre meine Arbeit sicherlich nicht so spannend geworden. Des weiteren möchte ich Henri Franquelim für die nützlichen Diskussionen über phasenseparierte Membranen, Sigrid Bauer für die Hilfe im Laboralltag, Grzegorz Chwastek für den Farbstoff ANEPP und Christoph Herold für das selbstgebaute TIRF Setup danken.

Selbständigkeitserklärung

Hiermit versichere ich, dass ich die vorliegende Masterarbeit erstmalig einreiche, selbständig verfasst und keine anderen als die angegebenen Quellen und Hilfsmittel verwendet habe.

Berlin - April 30, 2013